Geometric Symmetry Breaking and Nonlinearity Can Increase Thermoelectric Power

Jonatan Fast,[1,2] Hanna Lundström,[1,2] Sven Dorsch,[1,2] Lars Samuelson,[1,2,3] Adam Burke,[1,2] Peter Samuelsson,[1,4] and Heiner Linke[1,2]

[1]NanoLund, Lund University, Box 118, 22100 Lund, Sweden
[2]Solid State Physics, Lund University, Box 118, 22100 Lund, Sweden
[3]Institute of Nanoscience and Applications, Southern University of Science and Technology, Shenzhen, China
[4]Mathematical Physics, Lund University, Box 118, 22100 Lund, Sweden

(Received 28 February 2024; accepted 12 July 2024; published 11 September 2024)

Direct thermal-to-electric energy converters typically operate in the linear regime, where the ratio of actual maximum power relative to the ideal maximum power, the so-called fill factor (FF), is 0.25. Here, we show, based on fundamental symmetry considerations, that the leading order nonlinear terms that can increase the FF require devices with broken spatial symmetry. Studying nonlinear, thermoelectric transport across an asymmetric energy barrier defined in a single semiconductor nanowire, we find in both experiment and theory that we can increase the FF as well as maximum power. Geometric symmetry breaking combined with the design of nonlinear behavior thus represents a strategy for increasing the performance of thermoelectric or hot-carrier devices.

DOI: 10.1103/PhysRevLett.133.116302

Introduction—The ability to effectively convert heat stored in charge carriers into electricity is at the heart of existing and emerging technologies ranging from thermoelectric generators to hot-carrier photovoltaics and thermophotovoltaics. Generally, such devices operate in the linear-response regime where power output is fundamentally limited [1–3]: the so-called fill factor FF, which describes the shape of the current-voltage (I-V) curve in the power-producing quadrant, has the value FF $= 0.25$ by definition in the linear response regime. This means that the device's maximum power is four times smaller than the maximum power that corresponds to an ideal FF $= 1$ [4]. Optimizing the FF is a well-established strategy to increase the power output in photovoltaics, where a good silicon single-junction cell typically reaches FF ≈ 0.8 [5]. This strategy is, however, rarely considered in the context of thermal-to-electric energy conversion.

To achieve FF > 0.25 in thermal-to-electric energy conversion, it is necessary to introduce nonlinear I-V behavior. What nonlinear features are the most promising for increasing the FF? In the present work we show, based on fundamental symmetry considerations, that the leading order nonlinear terms that can increase the FF require devices that respond asymmetrically to the direction of external bias. This observation highlights device asymmetry as a critical attribute for increasing thermoelectric power. To experimentally demonstrate the role of broken symmetry, we study thermoelectric transport, in the nonlinear regime, across an asymmetric, ramp-shaped, energy barrier at temperature 77 K. The barrier is epitaxially defined by heterostructure engineering in a single semiconductor nanowire [Figs. 1(a)–1(c)]. The nanowire is equipped at either end with independent heaters that allow us to control the thermal bias in both directions along its axis [Figs. 1(d) and 1(e)]. We observe a large asymmetry in thermoelectric response with respect to the direction of thermal bias. Crucially, in one of the two configurations, we observe a FF > 0.25 that increases linearly in thermal bias, qualitatively consistent with theoretical predictions based on fundamental symmetry considerations. The strategy introduced here, to design device symmetry and its nonlinear behavior in order to increase the FF, offers new avenues for increasing the performance of thermal-to-electric energy converters. Importantly, this strategy is independent of and complementary to strategies to increase the traditional thermoelectric figure of merit ZT. ZT is a strictly linear-response quantity that holds no meaning for thermoelectric systems operating in nonlinear response regimes (see [6], Sec. VIII for a more detailed discussion of the relationship between FF and ZT).

Symmetry properties, nonlinear response, and fill factor—We begin by considering fundamental symmetry properties of a generic, n-type, two-terminal thermoelectric device driven by applying a thermal bias $\Delta T_{(\mathrm{L/R})}$ to the left (L) or the right (R) contact, respectively, resulting in an electrical current $I(V, \Delta T_{\mathrm{L}}, \Delta T_{\mathrm{R}})$. For heating at the right contact only $(\Delta T_{\mathrm{R}} = \Delta T > 0, \Delta T_{\mathrm{L}} = 0)$ the current can be

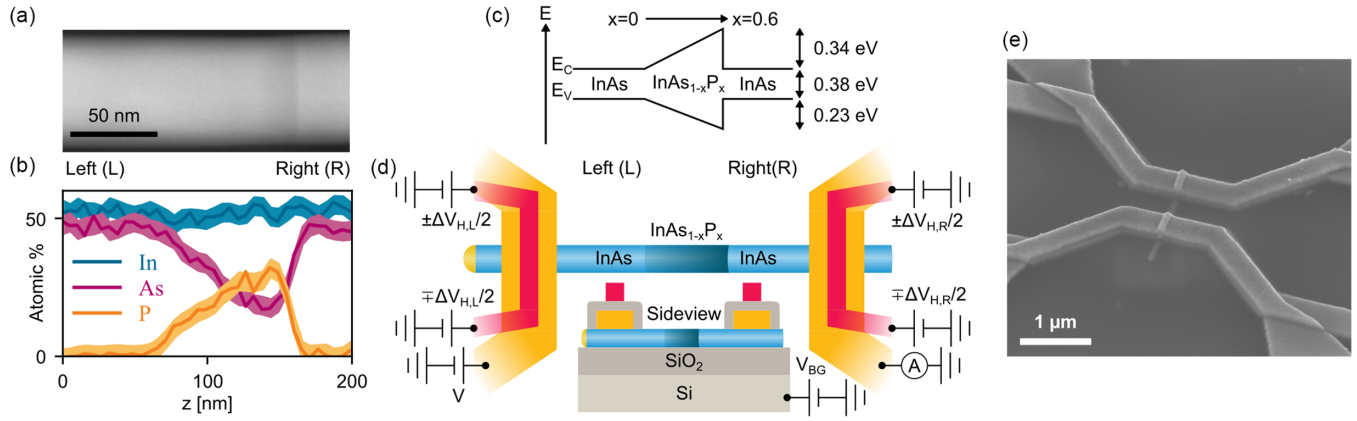

FIG. 1. (a) Scanning transmission electron microscope image and (b), energy-dispersive x-ray spectroscopy of a typical nanowire from the same growth as the studied nanowire, indicating the energy barrier shape. (c) Approximate, idealized, structure of the conduction (valence) band, E_C (E_V). (d) Device layout. A bias voltage V can be applied along the nanowire using the metallic leads (yellow). A heating voltage $\Delta V_{H,L}$ ($\Delta V_{H,R}$) can be applied on the left (right) side independently via the electrically insulated top heaters (red). The side view shows oxide layers for insulation on top of p-type Si for the application of a global back-gate voltage (V_{BG}). (e) Scanning electron micrograph of the completed device.

expanded to lowest nonlinear order in voltage and thermal bias as

$$I(V,0,\Delta T) = GV + L\Delta T + MV^2 + N\Delta T^2 + H_R V\Delta T, \quad (1)$$

where G, L, M, N, and H are constants describing the particular system. Heating instead at the left contact, assuming that heating by itself does not alter the device properties, that is $I(0,0,\Delta T) = -I(0,\Delta T,0)$, we can expand the current

$$I(V,\Delta T,0) = GV - L\Delta T + MV^2 - N\Delta T^2 + H_L V\Delta T. \quad (2)$$

For a spatially symmetric device it further holds that the current reverses sign under a simultaneous reverse of bias V and swapping of heating contact, that is

$$I(V,0,\Delta T) = -I(-V,\Delta T,0). \quad (3)$$

A symmetric device, fulfilling Eq. (3), constrains the expansion coefficients in Eqs. (1) and (2) to $M = 0$ and $H_L = H_R$. The fill factor is defined as $\mathrm{FF} = P_{max}/I_{SC}V_{OC}$, where P_{max} is the electrical power maximized with respect to V, I_{SC} the short-circuit current defined as the current at $V = 0$, and V_{OC} the open-circuit voltage. From the nonlinear current expressions in Eq. (1) and (2) we evaluate P_{max}, I_{SC}, and V_{OC} (see [6]). The resulting fill factor, expanded to lowest nonlinear order in thermal bias, is

$$\mathrm{FF}_{(L/R)} = \frac{1}{4} \mp \frac{ML}{8G^2}\Delta T, \quad (4)$$

with $+/-$ corresponding to heating at L/R, respectively. Hence, we can make our first key observation: for a spatially symmetric device ($M = 0$), to lowest order nonlinearity [Eqs. (1) and (2)], the fill factor continues to be restricted to its linear response value, $\mathrm{FF} = 0.25$. Increasing the FF of a thermoelectric system using leading order nonlinear behavior thus requires a system with broken spatial symmetry, such that $M \neq 0$, suggesting symmetry-breaking as a novel strategy for increasing the FF and thus thermoelectric power.

Observing asymmetric thermoelectric transport—How can one realize an asymmetric and nonlinear thermoelectric system in practice? One avenue is metallic superconducting systems, where a junction with electrodes with different superconducting gaps recently was shown to exhibit nonlinear thermoelectric effects at low temperatures [14,15]. In semiconductor devices, an asymmetric thermoelectric system has, to our knowledge, not been experimentally demonstrated. It is however well established that nonlinear thermoelectric systems can be realized in mesoscale devices [16–18], potentially with asymmetric behavior such as thermal rectification [19–22]. One approach to realize such systems is by varying the chemical composition of semiconductor materials at the nanometer scale in order to create potential barriers with energy selective transmission [23–26]. In semiconducting nanowires, such heterostructures can be synthesized with high control and precision [27–29].

Our experimental device consists of a single InAs nanowire with an $InAs_{1-x}P_x$ segment where the ratio of P to As is gradually increased to yield a ramp-shaped energy barrier, both in conduction and valence band, before abruptly transitioning back to InAs [Fig. 1(c)] [29]. We expect the carrier transport will be dominated by the behavior of electrons in the conduction band, as the chemical potential at InAs surfaces are known to be pinned in the conduction band [30,31]. The presence and shape of the heterostructure is confirmed by energy-dispersive x-ray

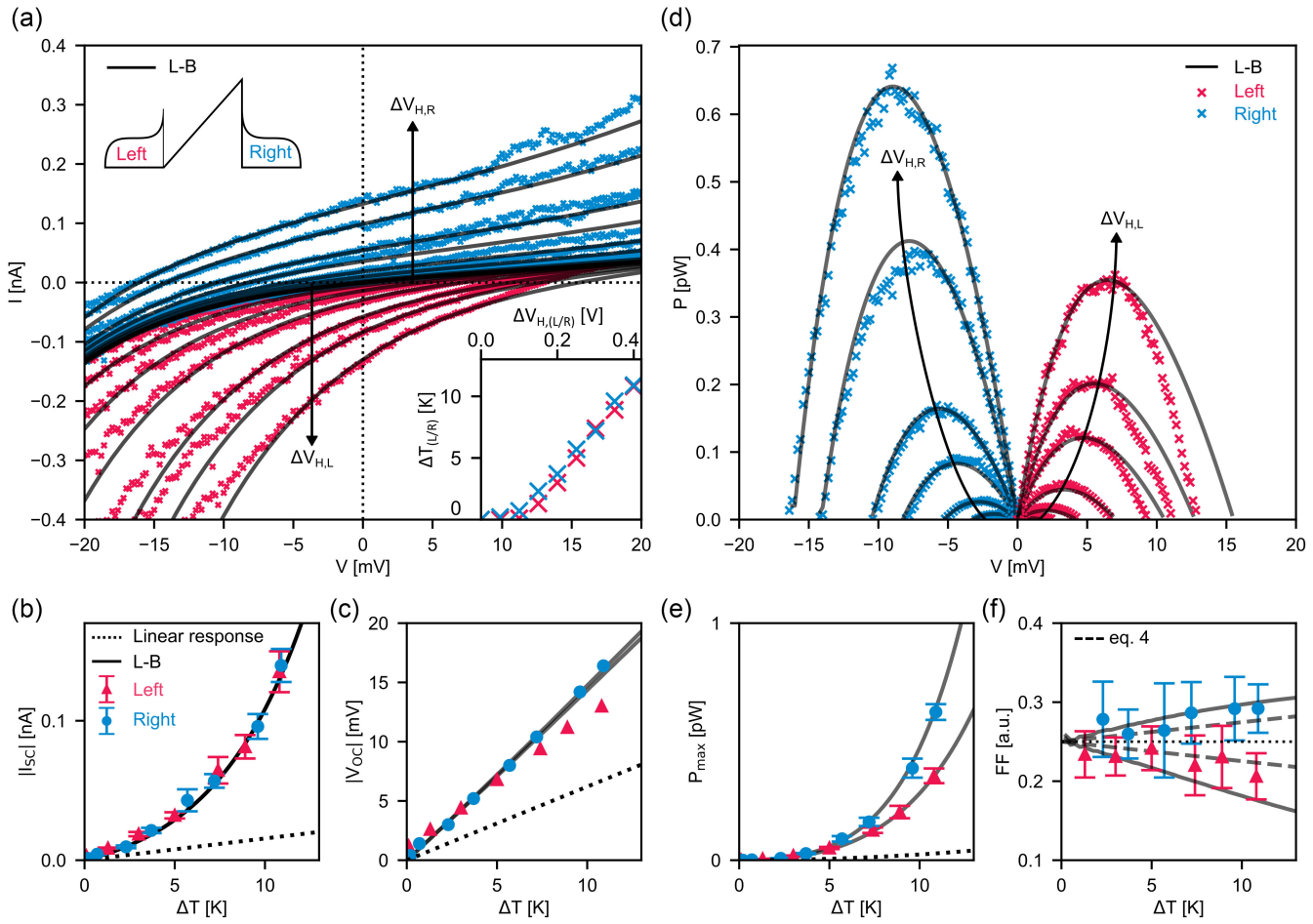

FIG. 2. (a) I-V curves while stepwise increasing the heating voltages $\Delta V_{\mathrm{H,R}}$ (blue marks), or $\Delta V_{\mathrm{H,L}}$ (red marks), respectively. Arrows indicate the direction curves shift for increasing ΔV_{H}. Each data point is the result of averaging 6 sweeps (standard deviations are shown in [6]). Solid black lines labeled L-B are calculated using Landauer-Büttiker theory [6] for barrier height $U_{\mathrm{top}} = 340$ meV, barrier length $L = 92$ nm, base temperature $T_0 = 77$ K, equilibrium chemical potential $\mu_0 = 100$ meV, and scaling factor $A = 710$ (see [6] for definition of A). The inset shows the relationship between ΔV_{H} and the resulting temperature bias ΔT, where values for ΔT are extracted from fits (see [6]) to I-V curves in (a). (b),(c) Short-circuit current I_{SC} and open-circuit voltage V_{OC} as a function of ΔT. Error bars indicate standard deviation, originating from the averaging of 6 sweeps (see [6]), which in (c) are smaller than the data point markers. (d) Power $P = |IV|$ in the power-producing quadrants as a function of V. (e),(f) Maximum output power P_{max} and fill factor FF as a function of ΔT. The experimental values for P_{max} are extracted from second order polynomial fits to curves in (d), see [6]. The dashed line in (f) shows FF calculated from Eq. (4) using the values for G, L, and M extracted from experimental data (see [6]). Dotted lines in (b),(c),(e),(f) show expected values under linear response, based on the extracted values for G and L.

spectroscopy [Fig. 1(b)]. Both ends of the nanowire are contacted by electrical leads, on top of which we place electrically insulated top heaters [32,33] [see Figs. 1(d) and 1(e)]. Applying a heating voltage ΔV_{H} to one of the top heaters generates Joule heat. The heat is transferred to the corresponding side of the nanowire via thermal conduction through the electric leads, resulting in a local increase of temperature ΔT. Using this design, thermal and electrical biasing can be applied independently from one another, and selectively in either direction across the barrier.

We define the left (L) and right (R) terminals of the device as the sides where the barrier has gradientlike shape, and a steep side, respectively [Figs. 1(c) and 1(d)]. Electrical bias is applied on the left side and current measured on the right, such that I is positive when electrons flow from R to L [Fig. 1(d)]. For thermal-bias measurements, ΔV_{H} is applied on either the left side ($\Delta V_{\mathrm{H,L}}$) or the right side ($\Delta V_{\mathrm{H,R}}$), resulting in a corresponding local temperature increase in the left ($\Delta T_{\mathrm{H,L}}$) or right ($\Delta T_{\mathrm{H,R}}$) end of the nanowire. The experiments were performed at a base temperature of $T_0 = 77$ K, meaning that the total temperature is given as $T_{(\mathrm{R/L})} = T_0 + \Delta T_{(\mathrm{R/L})}$.

We find that I-V curves in the absence of thermal bias ($\Delta V_{\mathrm{H,(L/R)}} = 0$) are nonlinear already at V of a few millivolts [Fig. 2(a)]. Increase of $\Delta V_{\mathrm{H,L}}(\Delta V_{\mathrm{H,R}})$ generates an additional negative (positive) thermal current, resulting in a

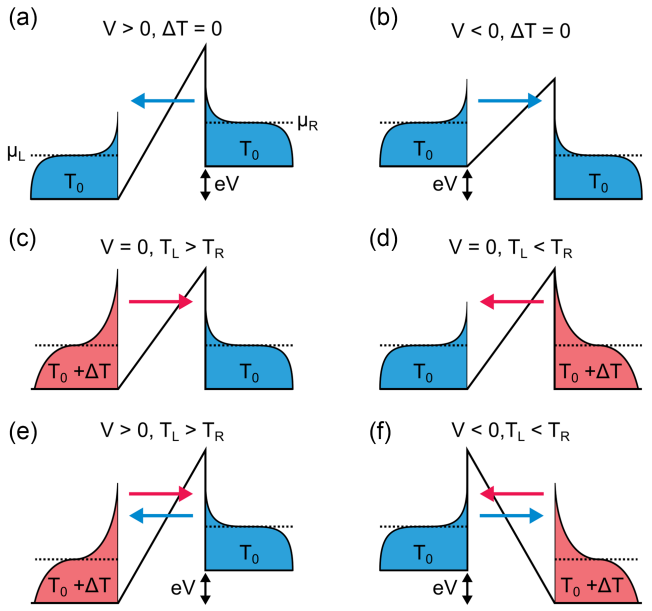

FIG. 3. Illustration of possible causes of the nonlinear effects and associated asymmetric behavior observed here. Blue and red colored regions illustrate Fermi-Dirac distributions. For consistent sign convention, it is assumed that the electrical bias is applied on the left side [as indicated in Fig. 1(d)]. (a),(b) Nonlinear effects originating from electrical bias during tunneling transport. An electrical bias V shifts μ by eV and causes electrons to flow to the side with lower μ, but alters also the barrier shape, such that $I(V) \neq -I(-V)$ for finite V. To lowest nonlinear order, these effects are described by $I = GV + MV^2$. (c),(d) Nonlinear effects originating from temperature-induced changes in the energy range of carriers participating in transport, described by the Fermi-Dirac distributions. Increasing temperature on one side causes electrons to flow to the colder side because electron transmission is higher at higher energy. To lowest nonlinear order, these effects are described by $I = L\Delta T + N\Delta T^2$. (e),(f) When producing power, the device is operated under both thermal and electrical bias, such that nonlinear transport of both origins may occur, and all five terms in Eqs. (1) and (2) are needed for the lowest nonlinear order description.

downward (upward) shift of the I-V curve. The sign of the thermal current indicates that heating on one side of the barrier results in a net electron flow to the opposite side. As $\Delta V_{\mathrm{H,L}}(\Delta V_{\mathrm{H,R}})$ is increased, the curve shape becomes more concave (convex) in the power-producing quadrant (the region between I_{SC} and V_{OC}). The change in curve shape suggests an increase in FF for heating on the right side, and a decrease in FF for heating on the left side.

To validate our results, and to determine the relation of ΔV_{H} to ΔT, we model the experiment within a Landauer-Büttiker scattering framework [34], fully incorporating nonlinear bias effects [35–37] (see [6]). Fits to the experimental data are found with strong agreement for all I-V curves [black solid lines in Fig. 2(a)], using a single set of parameters [see caption to Fig. 2(a)]. The good agreement of the fits provides evidence that the experimentally observed behavior is indeed due to the asymmetric barrier, and not, for example, due to imperfections in the nanowire. Furthermore, we can determine values for ΔT for each ΔV_{H} [inset to Fig. 2(a)]. The fit indicates an equilibrium chemical potential μ_0 on the order of 100 meV. Given the small experimental thermal energy of $k_{\mathrm{B}}T_0 \approx 7$ meV, electron energies E in all experiments reported here are thus expected to be well below the barrier top ($E < U_{\mathrm{top}}$), such that the device operates in the tunneling-transport regime.

Spatial asymmetry and nonlinearity can increase the fill factors—Importantly, the relationship between ΔV_{H} and ΔT indicates that the experimental heating arrangement operates symmetrically: we observe the same ΔT when $\Delta V_{\mathrm{H,L}} = \Delta V_{\mathrm{H}}$ and $\Delta V_{\mathrm{H,R}} = 0$, as when $\Delta V_{\mathrm{H,L}} = 0$ and $\Delta V_{\mathrm{H,R}} = \Delta V_{\mathrm{H}}$. Any observed asymmetries in the I-V curves are thus not expected to be related to unintentional asymmetries in the heater arrangement or performance. This observation is consistent with the symmetric behavior of I_{SC} [Fig. 2(b)]. At short-circuit conditions, and for symmetric heating, the response is expected to be symmetric with respect to the heating side irrespective of the direction of thermal bias, since the transmission probability across the barrier should be unchanged by temperature.

One main purpose of our study is to test whether device asymmetry and nonlinear behavior can be used to increase the FF beyond the linear response limit. To determine the experimental FF, we compared the ratio between the product $I_{\mathrm{SC}}V_{\mathrm{OC}}$ [Figs. 2(b) and 2(c)] to P_{max}, the maximum value of $P = |IV|$, for each ΔT [Figs. 2(d) and 2(e)]. Most interestingly, when heating terminal R we find a quasilinear fill-factor increase up to $\mathrm{FF} = 0.29 \pm 0.03$ at $\Delta T \approx 10$ K, an almost 20% improvement compared to the linear-response limit $\mathrm{FF} = 0.25$ [Fig. 2(f)]. When heating terminal L, we observe instead a corresponding decrease to $\mathrm{FF} = 0.21 \pm 0.03$. The observed quasilinear behavior of the FF with ΔT, as well as the observed splitting of FF with respect to heating direction, is in good qualitative agreement with the fundamental, lowest-order nonlinear prediction for a system where $M \neq 0$ [Eq. (4)].

To check for quantitative agreement with Eq. (4), we extract values for all coefficients in the generic nonlinear expansions of Eqs. (1) and (2). Details of this process are described in [6]. Briefly, G and M are extracted from I-V curves measured at $\Delta T = 0$ [Figs. 3(a) and 3(b)], L and N are extracted from $I(\Delta T)$ measured at $V = 0$ [Figs. 3(c) and 3(d)], and H is determined from measurements at finite V and ΔT in the linear response limit [Figs. 3(e) and 3(f)]. The origin of the corresponding nonlinear effects is illustrated in Fig. 3.

Using the values for M, L, and G, obtained in [6], Eq. (4) somewhat underestimates the observed FF splitting [dashed lines, Fig. 2(f)]. Comparison between Eq. (4) and the Landauer-Büttiker model, which includes full nonlinear behavior, indicates that about half of the experimentally

observed FF change is accounted for by the lowest-order nonlinear prediction [Eqs. (1) and (2)], whereas higher-order nonlinear terms account for the rest.

In addition to the change in FF, which describes a relative power, we also observe a drastic increase in absolute power as a function of ΔT [Fig. 2(e)]. The observed P_{max} in the nonlinear regime at $\Delta T = 10$ K ($\Delta T/T_0 \approx 13\%$) is up to 20 times higher than the $P_{\mathrm{max,lin}} = (L^2/4G)\Delta T^2$ predicted by the device's linear response properties [Fig. 2(e)]. The major part of this increase can be attributed to the clearly nonlinear behavior of I_{SC} [Fig. 2(b)], which in the observed range of ΔT is well described by $I_{\mathrm{SC}} = L\Delta T + N\Delta T^2$ (see [6]). A smaller portion of the increase can be attributed to an increase in V_{OC}, which also exceeds the linear response prediction $V_{\mathrm{OC}} = (L/G)\Delta T$ [Fig. 2(c)]. At $\Delta T = 10$ K, we find $V_{\mathrm{OC}}/\Delta T \approx 1.5$ mV/K, large compared to commonly observed Seebeck coefficients in linear response both in bulk and nanowire InAs [38–40].

Conclusion and outlook—We have shown that fundamental symmetry relationships dictate that samples with broken geometrical symmetry are a pre-requisite for observing leading-order nonlinear effects that could increase the thermoelectric FF. We also experimentally demonstrated the leading-order asymmetric change in FF predicted by Eq. (4) for an asymmetric device. This observation explains why nonlinear I-V curves are rarely observed in conventional thermoelectric systems, which typically are isotropic. Although transport across our ramp-shaped energy barrier was in the tunneling regime, where a very low current is expected, we nevertheless observe thermoelectric power on the order of 1 pW at $\Delta T \approx 10$ K, comparable to that observed in plain InAs nanowires of comparable quality and diameter at similar temperatures [41]. Future studies using different barrier shapes and varied μ_0 may be used to explore whether power production and FF can be further increased.

Importantly, our results suggest that improving the thermoelectric FF is a promising approach for creating more powerful thermoelectric devices and materials that can be pursued in addition to efforts to increase the traditional, linear-response ZT (see also [6] Sec. VIII). Looking to photovoltaic devices for inspiration, where a FF > 0.75 is not unusual, we can conclude that, for a given device or material, there is potential for an up to threefold increase in maximum power just based on FF, and more if nonlinear increases in I_{SC} and V_{OC} can be realized. In order to leverage the required nonlinear effects to leading order, devices with broken spatial symmetry must be used. There exists a wealth of systems that may be investigated to explore this design route for use in direct thermal-to-electric energy conversion. Examples include mesoscopic devices other than the one used in this study, including layered, two dimensional systems commonly used in hot-carrier photovoltaics [42–44]. A particularly promising candidate might be monolayers of asymmetric molecules [45,46]. Another route might be the design of anisotropic materials or metamaterials that combine asymmetry with nonlinear properties.

Acknowledgments—We thank M. Kumar for the synthesis of the nanowires, D. Madsen for the nanowire imaging with transmission electron microscope and compositional analysis with energy dispersive x-ray spectroscopy, and R. S. Whitney for valuable discussions. This work was supported by the Knut and Alice Wallenberg Foundation (Project No. 2016-0089), by the Swedish Research Council (Grant No. 2018-03921), and by NanoLund.

[1] G. Benenti, G. Casati, K. Saito, and R. S. Whitney, Fundamental aspects of steady-state conversion of heat to work at the nanoscale, Phys. Rep. **694**, 1 (2017).
[2] G. J. Snyder, Thermoelectric energy harvesting, in *Energy Harvesting Technologies*, edited by S. Priya and D. J. Inman (Springer, Boston, 2009), pp. 325–336.
[3] F. J. DiSalvo, Thermoelectric cooling and power generation, Science **285**, 703 (1999).
[4] G. Min, New formulation of the theory of thermoelectric generators operating under constant heat flux, Energy Environ. Sci. **15**, 356 (2022).
[5] L. Wang, Z. Q. Zhou, T. Zhang, and L. M. Chen X, High fill factors of Si solar cells achieved by using an inverse connection between MOS and PN junctions, Nanoscale Res. Lett. **11**, 453 (2016).
[6] See Supplemental Material at http://link.aps.org/supplemental/10.1103/PhysRevLett.133.116302 for a description of device characterization, measurement details, scattering model motivation, and parameter extraction by fitting of model to experiment, including Refs. [7–13].
[7] C. Hajlaoui, L. Pedesseau, F. Raouafi, F. B. C. Larbi, J. Even, and J.-M. Jancu, First-principles calculations of band offsets and polarization effects at InAs/InP interfaces, J. Phys. D **48**, 355105 (2015).
[8] S. Tiwari and D. J. Frank, Empirical fit to band discontinuities and barrier heights in III–V alloy systems, Appl. Phys. Lett. **60**, 630 (1992).
[9] G. Cliff and G. W. Lorimer, The quantitative analysis of thin specimens, J. Microsc. **103**, 203 (1975).
[10] D. B. Suyatin, C. Thelander, M. T. Björk, I. Maximov, and L. Samuelson, Sulfur passivation for ohmic contact formation to InAs nanowires, Nanotechnology **18**, 105307 (2007).
[11] C. Thelander, M. Björk, M. Larsson, A. Hansen, L. Wallenberg, and L. Samuelson, Electron transport in InAs nanowires and heterostructure nanowire devices, Solid State Commun. **131**, 573 (2004).
[12] R. G. Forbes and J. H. Deane, Transmission coefficients for the exact triangular barrier: An exact general analytical theory that can replace Fowler & Nordheim's 1928 theory, Proc. R. Soc. A **467**, 2927 (2011).
[13] R. H. Fowler and L. Nordheim, Electron emission in intense electric fields, Proc. R. Soc. A **119**, 173 (1928).

[14] G. Marchegiani, A. Braggio, and F. Giazotto, Nonlinear thermoelectricity with electron-hole symmetric systems, Phys. Rev. Lett. **124**, 106801 (2020).
[15] G. Germanese, F. Paolucci, G. Marchegiani, A. Braggio, and F. Giazotto, Bipolar thermoelectric Josephson engine, Nat. Nanotechnol. **17**, 1084 (2022).
[16] L. D. Hicks and M. S. Dresselhaus, Thermoelectric figure of merit of a one-dimensional conductor, Phys. Rev. B **47**, 16631 (1993).
[17] L. D. Hicks and M. S. Dresselhaus, Effect of quantum-well structures on the thermoelectric figure of merit, Phys. Rev. B **47**, 12727 (1993).
[18] A. Svilans, A. M. Burke, S. F. Svensson, M. Leijnse, and H. Linke, Nonlinear thermoelectric response due to energy-dependent transport properties of a quantum dot, Physica E (Amsterdam) **82**, 34 (2016).
[19] D. M.-T. Kuo and Y. C. Chang, Thermoelectric and thermal rectification properties of quantum dot junctions, Phys. Rev. B **81**, 205321 (2010).
[20] G. T. Craven, D. He, and A. Nitzan, Electron-transfer-induced thermal and thermoelectric rectification, Phys. Rev. Lett. **121**, 247704 (2018).
[21] K. Prakash, P. Thakur, S. Bansal, S. Garg, P. Jain, K. Sharma, N. Gupta, S. R. Kasjoo, S. Kumar, and A. K. Singh, Thermoelectric rectification in a graphene-based triangular ballistic rectifier (G-TBR), J. Comput. Electron. **20**, 2308 (2021).
[22] R. Scheibner, M. König, D. Reuter, A. D. Wieck, C. Gould, H. Buhmann, and L. W. Molenkamp, Quantum dot as thermal rectifier, New J. Phys. **10**, 083016 (2008).
[23] S. Kolenda, P. Machon, D. Beckmann, and W. Belzig, Nonlinear thermoelectric effects in high-field superconductor-ferromagnet tunnel junctions, Beilstein J. Nanotechnol. **7**, 1579 (2016).
[24] R. López and D. Sánchez, Nonlinear heat transport in mesoscopic conductors: Rectification, Peltier effect, and Wiedemann-Franz law, Phys. Rev. B **88**, 045129 (2013).
[25] M. Leijnse, M. R. Wegewijs, and K. Flensberg, Nonlinear thermoelectric properties of molecular junctions with vibrational coupling, Phys. Rev. B **82**, 045412 (2010).
[26] R. Wang, H. Liao, C.-Y. Song, G.-H. Tang, and N.-X. Yang, Linear and nonlinear thermoelectric transport in a quantum spin Hall insulators coupled with a nanomagnet, Sci. Rep. **12**, 12048 (2022).
[27] M. T. Björk, B. J. Ohlsson, T. Sass, A. I. Persson, C. Thelander, M. H. Magnusson, K. Deppert, L. R. Wallenberg, and L. Samuelson, One-dimensional heterostructures in semiconductor nanowhiskers, Appl. Phys. Lett. **80**, 1058 (2002).
[28] P. Caroff, M. E. Messing, B. M. Borg, K. A. Dick, K. Deppert, and L.-E. Wernersson, InSb heterostructure nanowires: MOVPE growth under extreme lattice mismatch, Nanotechnology **20**, 495606 (2009).
[29] G. Nylund, K. Storm, S. Lehmann, F. Capasso, and L. Samuelson, Designed quasi-1D potential structures realized in compositionally graded $InAs_{1-x}P_x$ nanowires, Nano Lett. **16**, 1017 (2016).
[30] C. A. Mead and W. G. Spitzer, Fermi level position at metal-semiconductor interfaces, Phys. Rev. **134**, A713 (1964).
[31] S. Bhargava, H.-R. Blank, V. Narayanamurti, and H. Kroemer, Fermi-level pinning position at the Au-InAs interface determined using ballistic electron emission microscopy, Appl. Phys. Lett. **70**, 759 (1997).
[32] J. G. Gluschke, S. F. Svensson, C. Thelander, and H. Linke, Fully tunable, non-invasive thermal biasing of gated nanostructures suitable for low-temperature studies, Nanotechnology **25**, 385704 (2014).
[33] A. Svilans, M. Leijnse, and H. Linke, Experiments on the thermoelectric properties of quantum dots, C. R. Phys. **17**, 1096 (2016).
[34] M. Büttiker, Four-terminal phase-coherent conductance, Phys. Rev. Lett. **57**, 1761 (1986).
[35] T. Christen and M. Büttiker, Gauge-invariant nonlinear electric transport in mesoscopic conductors, Europhys. Lett. **35**, 523 (1996).
[36] J. Meair and P. Jacquod, Scattering theory of nonlinear thermoelectricity in quantum coherent conductors, J. Phys. Condens. Matter **25**, 082201 (2013).
[37] D. Sánchez and R. López, Scattering theory of nonlinear thermoelectric transport, Phys. Rev. Lett. **110**, 026804 (2013).
[38] O. Madelung, U. Rössler, and M. Schulz, Group IV elements, IV-IV and III-V compounds. part b—electronic, transport, optical and other properties, 10.1007/b80447.
[39] A. Mavrokefalos, M. T. Pettes, S. Saha, Z. Zhou, and L. Shi, Combined thermoelectric and structure characterizations of patterned nanowires, in *Proceedings of the 2006 25th International Conference on Thermoelectrics* (2006), p. 234, 10.1109/ICT.2006.331248.
[40] Y. Tian, M. R. Sakr, J. M. Kinder, D. Liang, M. J. MacDonald, R. L. J. Qiu, H.-J. Gao, and X. P. A. Gao, One-dimensional quantum confinement effect modulated thermoelectric properties in InAs nanowires, Nano Lett. **12**, 6492 (2012).
[41] S. Roddaro, D. Ercolani, M. A. Safeen, S. Suomalainen, F. Rossella, F. Giazotto, L. Sorba, and F. Beltram, Giant thermovoltage in single InAs nanowire field-effect transistors, Nano Lett. **13**, 3638 (2013).
[42] J. A. R. Dimmock, S. Day, M. Kauer, K. Smith, and J. Heffernan, Demonstration of a hot-carrier photovoltaic cell, Prog. Photovoltaics **22**, 151 (2014).
[43] L. C. Hirst, R. J. Walters, M. F. Führer, and N. J. Ekins-Daukes, Experimental demonstration of hot-carrier photo-current in an InGaAs quantum well solar cell, Appl. Phys. Lett. **104**, 231115 (2014).
[44] Y. Harada, N. Iwata, S. Asahi, and T. Kita, Hot-carrier generation and extraction in InAs/GaAs quantum dot superlattice solar cells, Semicond. Sci. Technol. **34**, 094003 (2019).
[45] P. Reddy, S.-Y. Jang, R. A. Segalman, and A. Majumdar, Thermoelectricity in molecular junctions, Science **315**, 1568 (2007).
[46] H. Reddy, K. Wang, Z. Kudyshev, L. Zhu, S. Yan, A. Vezzoli, S. J. Higgins, V. Gavini, A. Boltasseva, P. Reddy, V. M. Shalaev, and E. Meyhofer, Determining plasmonic hot-carrier energy distributions via single-molecule transport measurements, Science **369**, 423 (2020).